Orbital Selective Mott Physics in Ca_2RuO_4

An angle resolved photo emission study

Fabio Cossalter

Supervised by: Denys Sutter

Supervising Professor: Johan Chang

Universität Zürich[UZH]

Department of Physics
University of Zurich
Switzerland
July 14, 2016

Abstract

In this bachelor thesis, the band structure of Ca_2RuO_4 is investigated and in particular efforts are made to assign orbital character to the observed bands. The band structure has been analysed by performing an Angle Resolved Photo Emission (ARPES) experiment. Performing a cut along high symmetry lines for different photon energies allows to observe variations in the spectral weight of different features of the ARPES spectra and subsequently assign a d_{xy} or $d_{xz,yz}$ character to these bands. Thus an argument for orbital selective Mott physics leading to Ca_2RuO_4's insulating state can be made, since the bands with different orbital character can be observed at different energy levels below the Fermi level.

Contents

Chapter 1

Introduction

In this thesis, the Mott insulating state of Ca_2RuO_4 has been investigated. It has been proposed, that an orbital selective Mott transition (see Figure 1.1) leads to the Mott insulating state [3], meaning that the different bands find themselves at different energy levels below the Fermi level. By studying the photon energy dependence of the different bands, one can determine the bands character. Here the photon energy dependence of the spectral weight of different bands has been evaluated, in order to determine their orbital character.

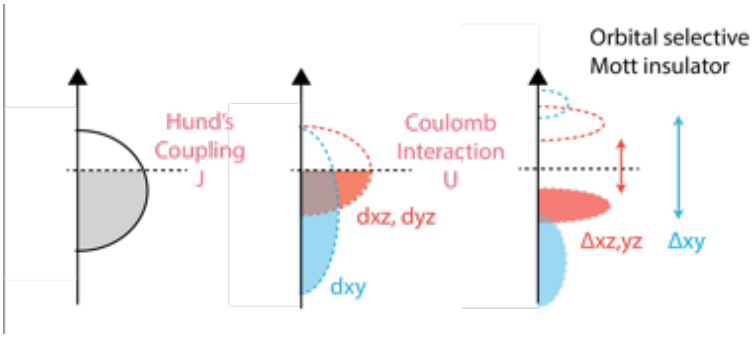

Figure 1.1: Proposed orbital selective behaviour of d_{xy},d_{xz} and d_{yz} bands of Ca_2RuO_4, different orbitals are subject to different transistions. The dotted line represents the Fermi level. The Hund's coupling leads to each orbital being subject to Coulomb interaction seperately, thus shifting them in different ways (see section 1.1). Adapted from [3].

1.1 Mott Insulator

I will limit myself at this point to explain Mott insulators in a phenomenological way. Ca_2RuO_4 is a strongly correlated electron system, interactions of the

electrons with themselves, i.e. Coulomb repulsion between particles with identical charge, can not be neglected. Thus the Mott insulator is a material which should conduct electricity when the band theory is applied, but does in fact not behave so. For depiction of a simple Mott insulator, see Figure 1.2. This thesis focuses on the orbital selective Mott insulator, meaning that the electrons in the different bands are, because of Hund's coupling enhancing orbital differentiation [13], subject to different levels of strength of Coulumb interaction, resulting in the bands being shifted differently below the Fermi level.

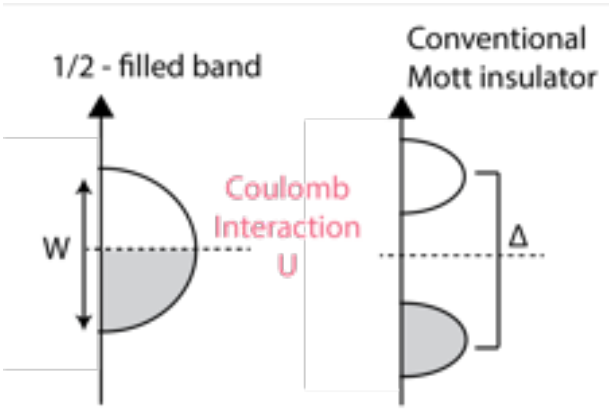

Figure 1.2: Mechanism of a conventional Mott insulator, the half filled band gets split up and shifted in it's respective energy level due to Coulomb interaction between the bands electrons. The grey band is now found below the Fermi level, indicated by the dotted line, showing a Mott gap between the grey band and the Fermi level.

1.2 Angle Resolved Photo Emission Spectroscopy (ARPES)

In photoemission spectroscopy electrons get ejected from a sample into a vacuum state because of the photoelectric effect, i.e. shining light on the sample. As described by Einstein [1], the following equation holds for this process:

$$\epsilon_{kin} = h\nu - \epsilon_B - \Phi \tag{1.1}$$

Here ϵ_{kin} is the ejected electrons kinetic energy in vacuum state, $h\nu$ is the energy of the incoming light quanta, ϵ_B is the electrons binding energy inside the sample and Φ denotes the samples work function, i.e. the energy required to eject the electron from the Fermi level into the vacuum state. For illustration of the process see Figure 1.3.

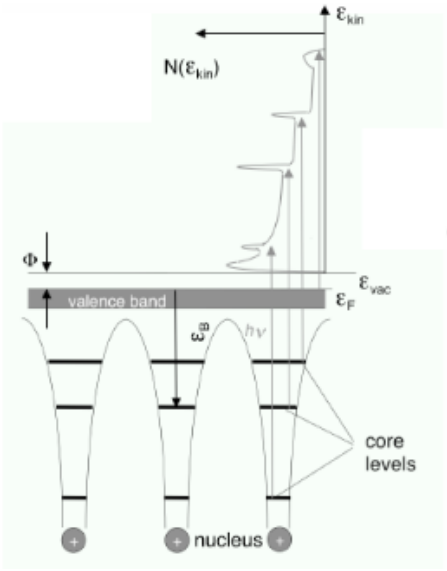

Figure 1.3: Illustration of the photoemission process, showing the parameters of Eq. 1.1, adapted from [7].

1.3 Intensity of ARPES-Signal

At this point a rather phenomenological understanding of how the intensity I of an ARPES signal comes together will be provided. In order to understand the photo emission process, a three step approach is used, adapted from [8]. At first an electron will be excited inside the sample by an incoming photon. Second, the electron will travel inside the sample, until it reaches its border. Finally the electron will leave the sample and find itself in a vacuum state.

First Step: We assume our sample to be a system of N electrons, from which one electron will get ejected by an incoming photon. This system of N electrons can be described by a wave function Ψ_α^N where $\alpha = \{i, f\}$ is the initial and final state of the system. According to the Hartree-Fock method, the following equation holds to describe our system.

$$\Psi_\alpha^N = \mathcal{A}\phi_\alpha^{\vec{k}}\Psi_\alpha^{N-1} \tag{1.2}$$

Here $\phi_\alpha^{\vec{k}}$ is the wave function of the ejected electron, Ψ_α^{N-1} is the wave function of the sample without the ejected electron and $\mathcal{A}$ is an antisymmetric operator, used to antisymmetrize the wave function, since we are dealing with fermions [8]. Now using first order, non stationary perturbation theory, the probability for the system to evolve from an initial state to a final state is given by Fermi's Golden Rule:

$$\Gamma_{i\to f} = \frac{2\pi}{\hbar}|\langle\Psi_f^N|H_{int}|\Psi_i^N\rangle|^2\delta(E_f - E_i - h\nu) \tag{1.3}$$

Here E_f is the samples final-state energy, E_i the samples initial-state energy, $h\nu$ is the incoming photons energy and H_{int} is the interacting Hamiltonian between the electron that gets ejected and the incoming photon. H_{int} is derived via the interaction Hamiltonian between matter and radiation.

$$H = \frac{1}{2m}(\boldsymbol{p} - \frac{e}{c}\boldsymbol{A}(\boldsymbol{r}))^2 = H_0 + H_{int} \tag{1.4}$$

Here $\boldsymbol{A}(\boldsymbol{r})$ is the vector potential of the radiation and $\mathbf{p}$, $\mathbf{r}$ are the electrons momentum and position. Solving Eq. 1.4 for H_{int} gives us the interacting Hamiltonian.

$$H_{int} = -\frac{e}{2mc}(\boldsymbol{p}\cdot\boldsymbol{A}(\boldsymbol{r}) + \boldsymbol{A}(\boldsymbol{r})\cdot\boldsymbol{p}) + \frac{e^2}{2mc^2}\cdot\boldsymbol{A}(\boldsymbol{r})^2 \tag{1.5}$$

Since we are looking at first order perturbation theory, the term proportional to $\boldsymbol{A}(\boldsymbol{r})^2$ can be neglected, further we can safely assume that $\boldsymbol{A}(\boldsymbol{r}) = const.$ for atomic distances, thus $\nabla\cdot\boldsymbol{A} = 0$. This leads to the conclusion that the comutator $[\boldsymbol{p}, \boldsymbol{A}] = 0$. Taking this into account, the interacting Hamiltonian H_{int} can be simplified as follows:

$$H_{int} = \frac{e}{mc}\boldsymbol{A}\cdot\boldsymbol{p} \tag{1.6}$$

Since we are assuming that only one electron gets ejected, it is safe to say that the interacting potential H_{int} just acts on the initial single electron state, described by the wave function $\phi_i^{\vec{k}}$. Therefore the matrix element of the transition probability, found in Fermi's Golden Rule (Eq. 1.3), can be factorized in the following way:

$$\langle\Psi_f^N|H_{int}|\Psi_i^N\rangle = \langle\phi_f^{\vec{k}}|H_{int}|\phi_i^{\vec{k}}\rangle\langle\Psi_f^{N-1}|\Psi_i^{N-1}\rangle \tag{1.7}$$

Here the term $\langle\phi_f^{\vec{k}}|H_{int}|\phi_i^{\vec{k}}\rangle$ is the one-electron dipol matrix element which we denote from here on as $M_{f,i}^{\vec{k}}$. The one-electron dipol matrix element connects the electron emissioned by the photon with this electrons intital state in the N electron system. The term $\langle\Psi_f^{N-1}|\Psi_i^{N-1}\rangle$ is the $(N-1)$ electron overlap integral. Since our sample Ca_2RuO_4 is a strongly correlated electron system, the overlap integrals are generally different from zero, so one has to solve a lot of them in order to derive the intensity. Because of that, a different approach has been chosen, using the spectral function $A(\vec{k}, E)$ instead. The spectral function $A(\vec{k}, E)$ basically describes the excitation of the system when one electron is removed. Since the spectral function contains many different forms of interaction, the calculation of it is rather complex and I will limit myself in this thesis to just present the equation:

$$A(\vec{k}, E) = -\frac{1}{\pi} \frac{\Im\Sigma(\vec{k}, E)}{[E - \epsilon(\vec{k}) - \Re\Sigma(\vec{k}, E)]^2 + [\Im\Sigma(\vec{k}, E)]^2} \tag{1.8}$$

By looking at Eq. 1.8 we can see that the spectral function $A(\vec{k}, E)$ can be compared with the function

$$f(x) = \frac{1}{\pi} \frac{s}{s^2 + (x - x_0)^2} \tag{1.9}$$

the probability density function of a cauchy distribution, with s being the scale parameter, describing half width at half maximum and x_0 describing the location of the peak. Thus the spectral function $A(\vec{k}, E)$ has a lorentzian line shape. The spectral function $A(\vec{k}, E)$ includes the parameters E, the excitation energy of the system, with $E = 0$ describing the Fermi level, $\epsilon(\vec{k})$, the band energy of the non interacting electron, given by:

$$\epsilon(\vec{k}) = \frac{\hbar^2 \vec{k}^2}{2m} \tag{1.10}$$

and $\Sigma(\vec{k}, E)$, the particles self energy, i.e. the energy of the particle taking its interaction with the system it is part of into account. The real part $\Re\Sigma(\vec{k}, E)$ describes the renormalization of the energy of the $(N-1)$ particle system due to the removal of one electron and the imaginary part $\Im\Sigma(\vec{k}, E)$ describes the inverse electron lifetime and is thus proportional to s of the cauchy distribution. We are now able to express the intensity of the ARPES signal in the following way:

$$I(\vec{k}, E) = I_0(\vec{k}, \nu, \boldsymbol{A}) f(E) A(\vec{k}, E) \tag{1.11}$$

Here the term $I_0(\vec{k}, \nu, \boldsymbol{A})$, depending on the vector $\vec{k}$, the photon frequency ν and the vector potential $\boldsymbol{A}$, is proportional to the matrix element $M_{f,i}^{\vec{k}}$. The term $f(E)$ represents the Fermi-Dirac distribution

$$f(E) = \frac{1}{e^{\frac{E - E_F}{k_B T}} + 1} \tag{1.12}$$

accounting for the fact, that just occupied states will be probed.

Second Step: Now that the electron got ejected from its inital state in the N electron system it has to travel to the samples surface. On its way to the surface, the electron mainly interacts via inelastic electron-electron scattering. By assuming that these scattering processes have roughly the same probability at any time of the electrons travelling, one can describe the mean free path by using the universal curve (Eq. 1.13), which is material independent, thus the mean free path only depends on the electrons energy.

$$I(x) = I_0 e^{\frac{-x}{\lambda(E)}} \tag{1.13}$$

Here I_0 is the intensity of at the beginning of the travel, x is the distance and $\lambda(E)$ is the electrons inelastic mean free path, depending only on its energy E.

Third Step: Crossing the samples surface and reaching a vacuum state, the electron has to compensate for the surface potential ϕ, thus, for being ejected from the sample, the electron needs to have sufficient energy to both reach its surface and to overcome the work potential ϕ at the surface.

Limitations: In order for the three step model to be plausible, certain approximations were made. For example in the second step, the process of the electron travelling to the samples surface is described only by the parameter E, since the inelastic mean free path $\lambda(E)$ (see Eq. 1.17) is given in the following way:

$$\lambda(E) = \frac{143}{E^2} + 0.054 \cdot \sqrt{E} \tag{1.14}$$

It is also assumed that the so called *sudden approximation* holds, meaning that many body interactions and relaxation of the system during the photo emission process is neglected.

Chapter 2

Experiment

2.1 Basic Properties of Ca_2RuO_4

The sample Ca_2RuO_4 is a member of the alloy series $Ca_{2-x}Sr_xRuO_4$, choosing $x = 0$. Furthermore, Ca_2RuO_4 behaves as a Mott insulator [2],[3] (see section 1.1.) The crystal structure is made up of RuO_2 layers built up of cornersharing RuO_6 octahedra, belonging to space group Pbca [12]. For illustration see Figure 2.1.

The crystal has a orthorombic structure with lattice constants $a = b \approx 5.4$ Å and $c \approx 11.9$ Å, since the next neighbour for the tetragonal unit cell is tilted. The approximation symbol is used because the lattice constants vary with changing temperature [4]. The electronic structure of Ca_2RuO_4 is composed of d_{xy}, d_{xz} and d_{yz} orbitals [3], for illustration of the orbitals see Figure 2.2.

2.2 Experimental setup at I05 Beamline

The ARPES measurments were done at the I05 beamline of the Diamond Lightsource (DLS) at Harwell Campus near Oxford, UK. For a schematic illustration of the experimental setup, see Figure 2.3.

The undulator is creating the photon beam by sending electrons through a tunnel of alternating magnetic fields, thus accelerating charge and therefore creating the photon flux. The white light created by the undulator then gets monochromatized by a collimated plane grating monochromator consisting of the vertical collimating mirror M1, the plane mirror M2 and a diffraction grating. The beam then gets focused on target by the cylindrical mirrors M3 and M6. The beam travels a total of 50 m until it reaches the target. The photon energy can be chosen from a range of $18 - 240$ eV, the instruments energy resolution is 10 meV and the angular resolution is 0.1° [6]. After hitting the target, ejected electrons will enter the analysing device, shown in Figure 2.4.

By applying a voltage between the inner and outer sphere of the analyser, thus creating an electric field in the curve, one can choose the energy range of

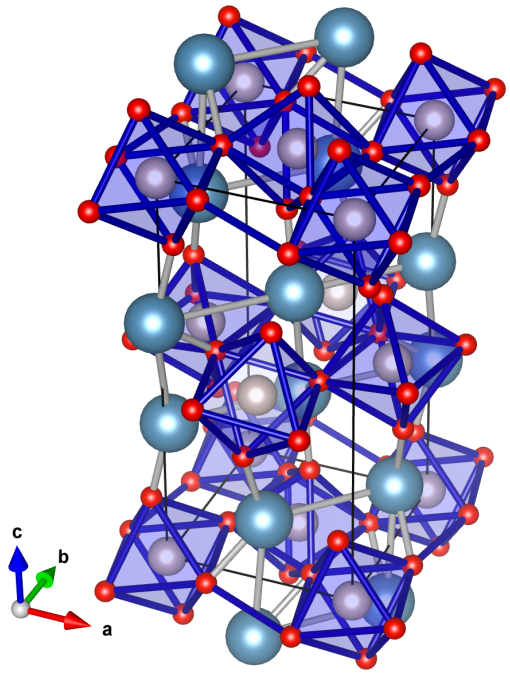

Figure 2.1: Crystal structure of Ca_2RuO_4, belonging to the space group Pbca, the grey spheres represent the Ru atoms, the red spheres represent the O atoms and the blue spheres represent the Ca atoms.

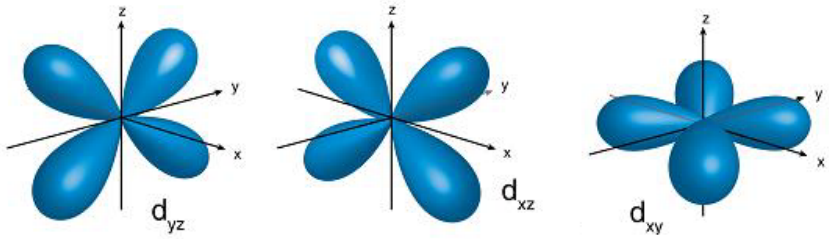

Figure 2.2: Visualization of the d_{yz}, d_{xz}, d_{xy}-orbitals, adapted from [5].

the electrons reaching the CCD camera, where they get detected. If an electron has too little energy, it will hit the inner sphere, whereas it will collide with the outer sphere if it has abundant energy. The CCD camera basically consists of linear arranged detector channels, thus giving information about $\vec{k}$ of the emitted electron, see Figure 2.5 for further illustration.

To put the sample in the beamline, four vacuum chambers had to be passed.

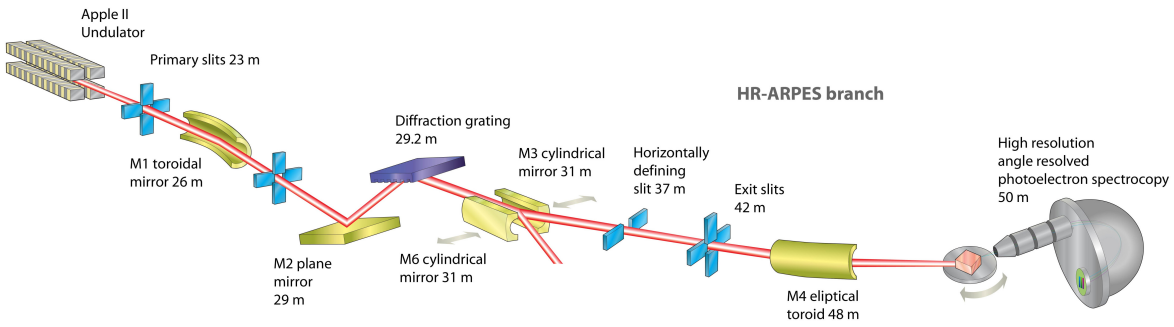

Figure 2.3: Beamline layout for the I05 ARPES endstation at Diamond Light Source in Oxford, adapted from [6].

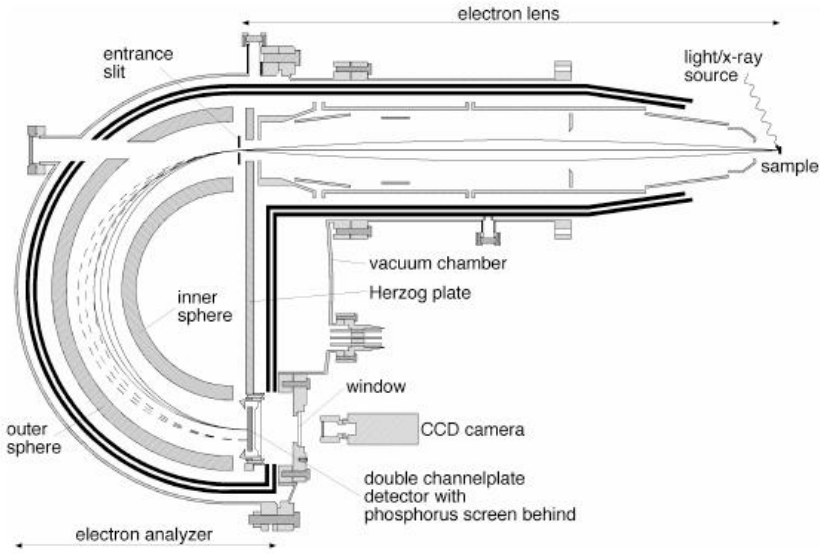

Figure 2.4: Electron analyser of ARPES setup, adapted from [7].

First the sample gets inserted and put on a rail like device which can store about eight samples. This device then gets transfered to the second chamber, where one sample from the rail gets selected. In the third chamber, the sample gets installed in the manipulator of the experiment and after that, once the decided temperature is achieved, the sample will be cleaved (see section 2.3). Finally the sample gets transfered to the fourth chamber, where it will get exposed to the beam. The vacuum in the first chamber has an order of magnitude of about 10^{-8} mbar, whereas it will then get lowered in the subsequent chambers to an

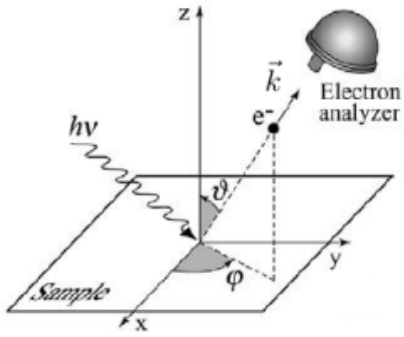

Figure 2.5: Geometry of ARPES, where ϑ is the polar and φ is the azimutal angle and the electrons movement is described by the vector $\vec{k}$, adapted from [8].

order of magnitude of about 10^{-10} mbar. In the first chamber, nitrogen was inserted, since it supports the pump out speed. The sample was analysed at a temperature of $T \approx 150$ K and for the photon energy dependence measurements circular righthanded polarized light was used.

2.3 Sample preparation

Beforehand: The batch of crystals was grown in Salerno. The first step was to select crystals with a nice surface. After that, the crystals were glued on the sample holder made of the copper alloy phosphor bronze by using the conducting glue Epoxy (EPO-TEK E4110), which is a two component, electrically conductive, silver filled epoxy paste [9]. The epoxy is used since performing ARPES with an insulating material will result in the sample getting charged, thus distorting the results. The conducting epoxy can prevent this charging. In a next step, the sample got aligned by using a Laue X-Ray device, working at a beam voltage of 39.6 kV and a beam current of 0.307 mA. For further illustration of the Laue process, see Figure 2.6. The orientation was then indicated by drawing two points with epoxy on the sample holder. In a further step, the samples were cleaned in two steps, utilising ethanol and acetone respectively, using an EMAG Emmi-40HC ultrasound cleaning device. Finally, a pin was glued on the sample, in order to be able to cleave it on site in the third vacuum chamber.

On Site: At first, graphite was put on the sample in order to enhance its conductivity and to decrease the background noise caused by the phosphor bronze sample holder. At last, the sample was cleaved in the third vacuum chamber, using an already installed manipulator. Also there was a removable tray prepared where the removed pin could fall on. The cleaving of the sample ensures a proper surface on the sample and is made possible by the Ca_2RuO_4

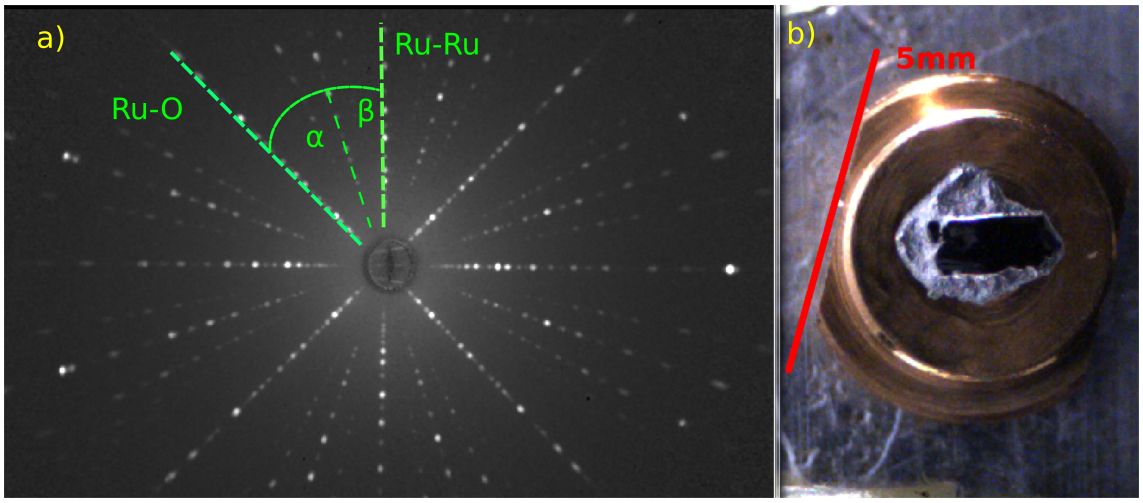

Figure 2.6: a) Laue picture of a sample, having used an exposure time of $300s$. The fact that the angles α and β are not equal has been used to align the sample [10]. b) Picture of the sample in a position corresponding to the Laue image. The black object in the middle is the sample, lying on the silver epoxy. The red line is used to give some sense of proportion.

structure, which consists of two layers and is therefore highly 2-dimensional (see 2.1). The parameter of the cleaving is the amount of glue one uses. With too little glue applied, the sample will not cleave properly and one remains with a polluted surface. Too much glue on the other hand will cause the whole sample to be detached from the sample holder.

Chapter 3

Data Analysis

3.1 Calibration of ARPES Spectra

The raw data output of the ARPES experiment at DLS consists of 2-dimensional matrices. Each column entry corresponds with a detector cell. The detector at the I05 beamline has 690 cells, i.e. the matrices have the dimension $x \times 690$. Each row corresponds to measuring the intensity detected for a given kinetic energy of the signals electrons, which the experimentator can choose (see section 2.2). For analysing the $h\nu$ - dependence mostly 626 energy steps were made. This leaves us with 626×690 matrices filled with intensities in arbitrary units. We know E_{kin} for each row and the angles can easily be deduced by knowing the total angle covered by the detector and the number of detector cells. Visualizing the raw output leads us to Figure 3.1.

Now two calibration steps need to be taken. The energy scale will be converted to the binding energy scale and the angles will be converted to k-space. First we take a look at the conversion of the energy scale. The binding energy E_B can be determined via the formula:

$$-E_B = E_{kin} - E_F \tag{3.1}$$

Here E_{kin} is the kinetic energy, given by the raw data, and E_F is the Fermi energy that needs to be determined. The Fermi energy is evaluated by using a gold reference, getting the fermi level there and project it to the Ca_2RuO_4 sample. For illustration of the gold, see Figure 3.2.

Here the intensities in each column get integrated and then fitted with the Fermi function (see Eq. 1.12), see Figure 3.3.

Now the binding energy E_B can be determined via Eq. 3.1. At this point it is also possible to derive the experiments energy resolution ΔE. From the Fermi fit we get the temperature T_{FD}, the Fermi Dirac temperature, and we can connect it with ΔE via the equation:

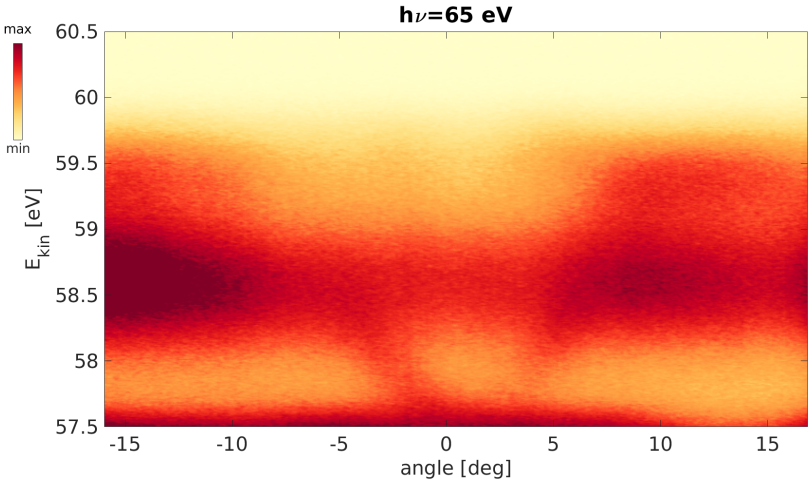

Figure 3.1: Raw data of ARPES experiment, performing a Γ-S cut (see section 3.1.1).

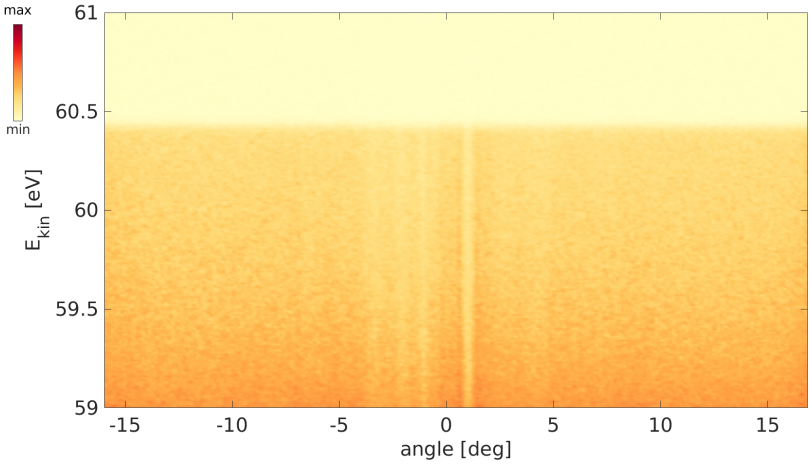

Figure 3.2: Intensities of gold reference, with clear rise of intensity at $E_{kin} \approx$ 60.5 eV.

$$T_{FD} \cong \sqrt{(T_{sample})^2 + (\frac{\Delta E}{4k_b})^2} \tag{3.2}$$

Here $T_{FD} = 148$ K is extracted from the fit parameter, $T_{sample} = 150$ K is known from the experiment and k_b is the Boltzmann constant. We can now solve Eq. 3.2 for the energy resolution ΔE.

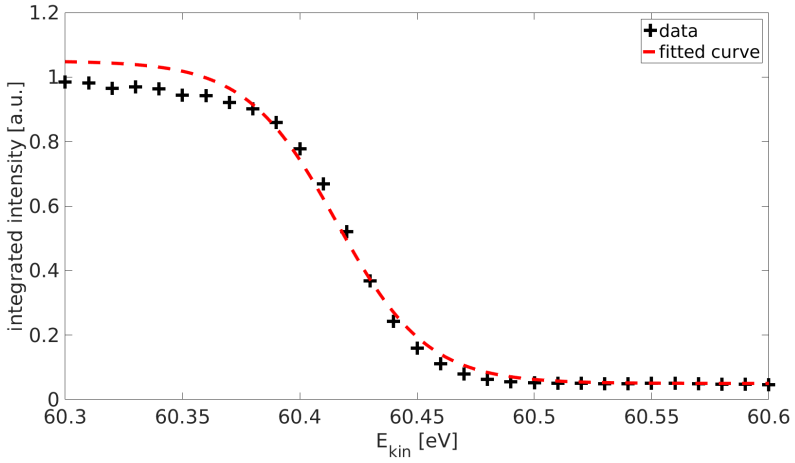

Figure 3.3: Integrated intensites of gold fitted with the Fermi function, fixing the Fermi energy at $E_F = 60.4$ eV.

$$\Delta E \cong 4k_b\sqrt{(T_{FD})^2 - (T_{sample})^2} \tag{3.3}$$

This leads to an energy resolution of $\Delta E \cong 72$ meV. Next the angles need to be converted to k-space. By looking at Figure 2.5 one can derive that the crystal momentum $\vec{k} = \frac{\vec{p}}{\hbar}$ is given by the equation (using Eq. 1.10):

$$\vec{k} = \frac{\sqrt{2mE_{kin}}}{\hbar}(sin\vartheta, 0, cos\vartheta) \tag{3.4}$$

Here the angle ϑ corresponds to the one in Figure 2.5. Note that Eq. 3.2 is only true for the laboratory system. Since it is possible to put the manipulator, where the sample lies on, on an angle, one has to consider this as well. In this case, the method found in [10] was applied to transform $\vec{k}$ to the laboratory system. We are now able to visualize as shown in Figure 3.4.

3.1.1 Orientation in the unit cell

All cuts discussed in this thesis were made from the Γ to the S point of the orthorombic Brioullin zone. Making a cut means here orienting the slit of the CCD camera so that it is aligned with the Γ-S direction in the orthorombic Brioullin zone. The orthorombic Brioullin zone is chosen since the next neighbour for the tetragonal zone is tilted and is therefore not a real neighbour (see Figure 2.1). For illustration of the Brioullin zone see Figure 3.5.

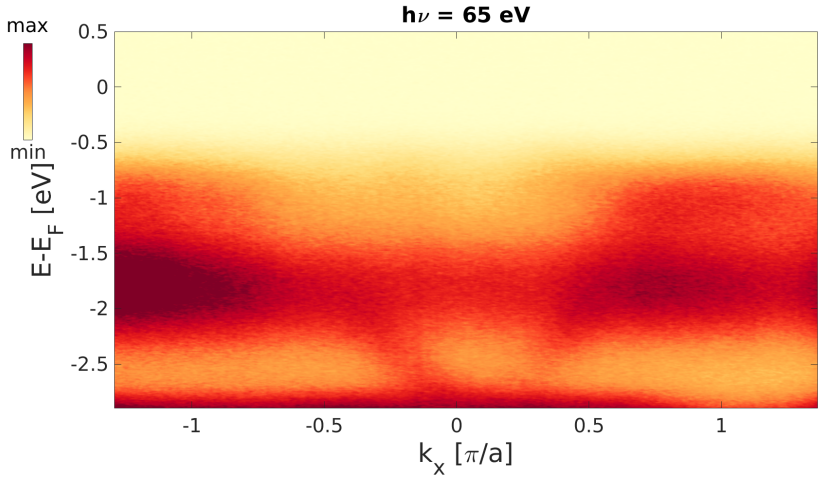

Figure 3.4: Calibrated data, the y-axis is in the binding energy scale, the x-axis in k-scale in units of $\frac{\pi}{a}$, where a is the lattice constant.

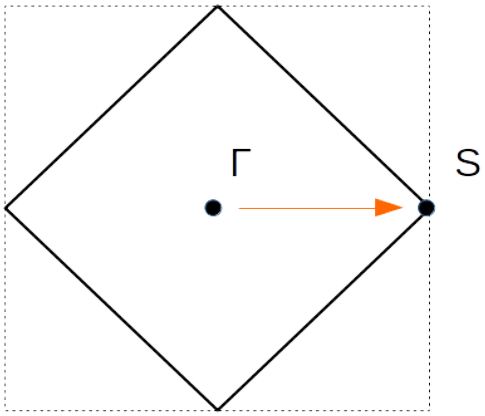

Figure 3.5: Illustration of the tetragonal unit cell (dotted line) and the orthorombic unit cell (drawn out line), the red vector indicates the cut.

3.2 Analysis of ARPES Spectra

3.2.1 Integration of Signal for Different Photon Energies $h\nu$

In order to study the photon energy dependence of the features, for example the fast dispersing band around $k_x = 0$ (see Figure 3.4), it was chosen to intergrate

the signal bounded by a box, whichs placing and size can be chosen. Since the data gathered at DLS is subject to a shift in the Fermi level, charging of the sample is expected to have happened (see Figure 3.6). Therefore a set of data gathered at the SIS beamline at the Paul Scherrer Institut (PSI) in Villigen, AG is considered from here on, which has not been subject to charging.

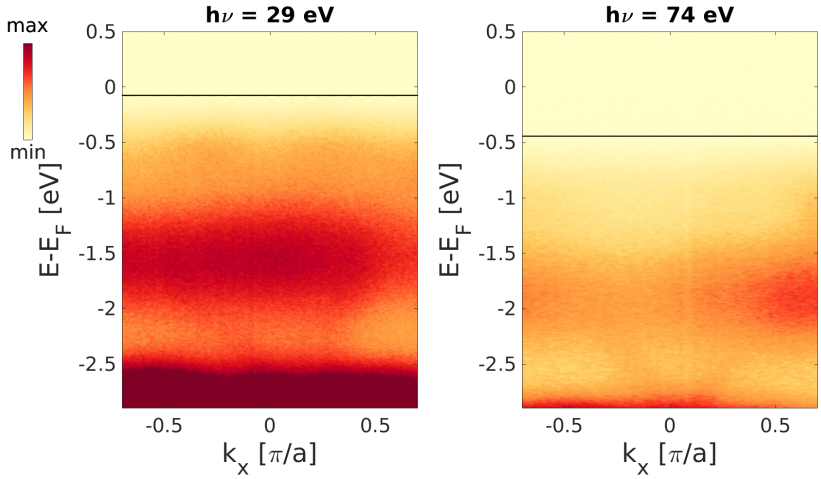

Figure 3.6: Plot of beginning and ending photon energy of the DLS data, the horizontal black line indicates the shift in the Fermi level.

Using matlab for data analysis easily allows to select a window of a given matrix for a particular photon energy. All entries in this window then were summed up, thus providing the integrated intensity of the area bounded by the before mentioned box (see Figure 3.7).

In Figure 3.7 the following intensities (in arbitrary units) were measured for the boxes:

$$I_{blue} = 1474486$$

$$I_{green} = 1489510$$

This process has been done iteratively, covering photon energies from 30 eV - 81 eV in steps of 3 eV. In contrast to the DLS data, the PSI data consists of 3-dimensional matrices, where the third dimension indicates the given photon energy, therefore the scripts had to be adapted to this fact.

3.3 Results

The results are visualized in Figure 3.8, Figure 3.9 and Figure 3.10. It can be observed that both features in focus show some photon energy dependence, but

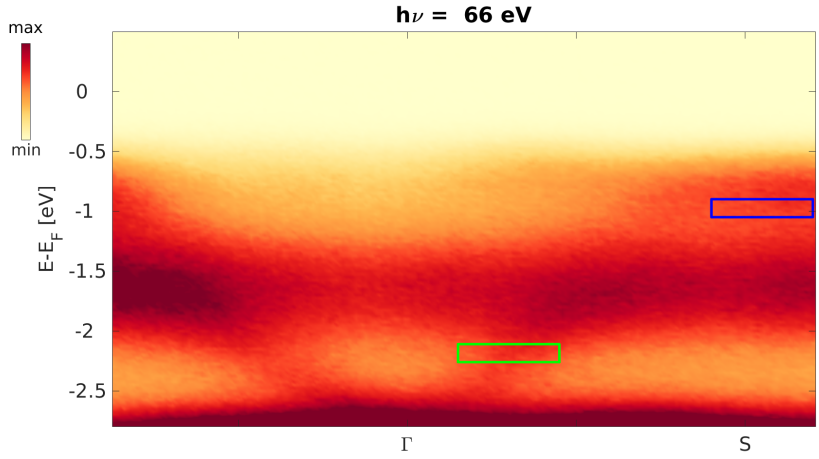

Figure 3.7: ARPES spectrum of the PSI data at a photon energy of $h\nu = 66$ eV, the blue and green box show the area where the intensity has been integrated.

the dependence of the feature in the blue box seems to be much stronger. The feature at an energy level of $E\text{-}E_F \approx$ -2.3 eV has a more or less linear decrease in intensity with increasing photon energy. The feature at an energy level of $E\text{-}E_F \approx$ -1 eV shows a minimum around a photon energy of 45 eV and a maximum around a photon energy of 60 eV. As it will be shown in Chapter 4, these results are in good agreement with our expectations and are now used to support the claim for orbital selective Mott physics as a reason for Ca_2RuO_4's insulating state. For further analysis, including an angular correction method and some background calculations of the DLS data I may point here to the appendix.

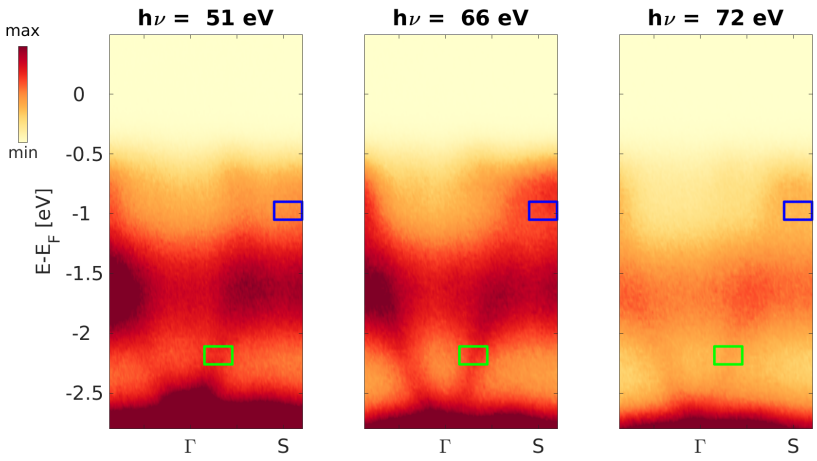

Figure 3.8: ARPES spectra with boxes indicating the integrated areas, three photon energies have been picked out.

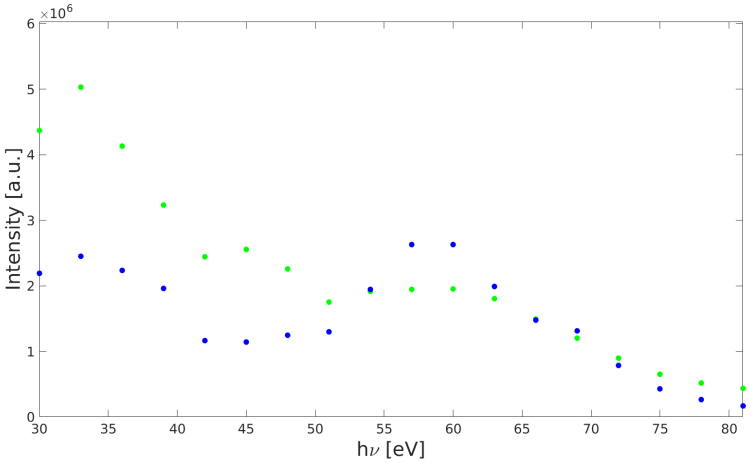

Figure 3.9: Plot of the integrated intensities versus the photon energy, the green dots correspond with the green box and vice versa.

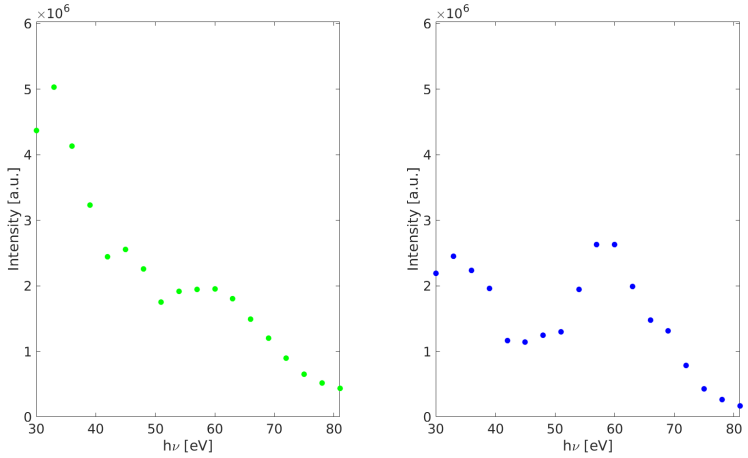

Figure 3.10: Integrated intensities versus photon energy, same correspondence as in Figure 3.9. Here the plots are seperated for better visualization of the individual behaviour.

Chapter 4

Conclusions

From the results it is evident that different features of the ARPES spectra are being either strongly or weakly impacted by a change in photon energy. One can now use this fact to identify the feature in focus as having d_{xy} or $d_{xz,yz}$ orbital character. We can write the matrix element of Eq. 1.11 in the following way [11]:

$$M = \sum_{\delta} (M_x^{\delta} + M_y^{\delta} + M_z^{\delta} e^{i\gamma}) \tag{4.1}$$

Here $\delta = \{d_{xy}, d_{xz}, d_{yz}\}$ and $\gamma = k_z c$, where c is the lattice constant in z direction. The phase $e^{i\gamma}$ has an experimentally derived value and accounts for the stacking of the planes of Ca_2RuO_4. Now each component of Eq. 4.1 can be evaluated seperately, choosing the ansatz [3]:

$$M_i^{\delta} = A_i \Upsilon_i^{\delta} \tag{4.2}$$

Here $i = \{x, y, z\}$ and $\vec{A}$ is the light polarization vector. Υ_i^{δ} contains the radial and angular solutions of Schrödingers equation plus a Bessel function and Gaunt coefficients. Since the radial part of the solution of Schrödingers equation depends in this case on a Coulomb potential of the form $V(r) = -\frac{Ze^2}{r}$, one has to choose a value for the atomic number Z, i.e. the number of protons, here $Z = 20$ was chosen. Evaluating this, it is found that d_{xy} orbitals are not subject to oscillations, since $M_z^{d_{xy}} = 0$ and the $d_{xz,yz}$ bands are bound to oscillate more strongly when changing the photon energy, thus depending on k_z. The theoretical calculation is depicted in Figure 4.1 and is in good agreement with the obtained data.

It is now possible to identify the fast dispersing band around $E_B \approx -2.3$ eV as having d_{xy} orbital character, whereas the bands at $E_B \approx -1$ eV are having a $d_{xz,yz}$ orbital character. This approach is justified by the fact that for 3d metallic systems, such as pnictide superconductors, an oscillation of the spectral weight of the $d_{xz,yz}$ bands has been observed [11]. The approach has

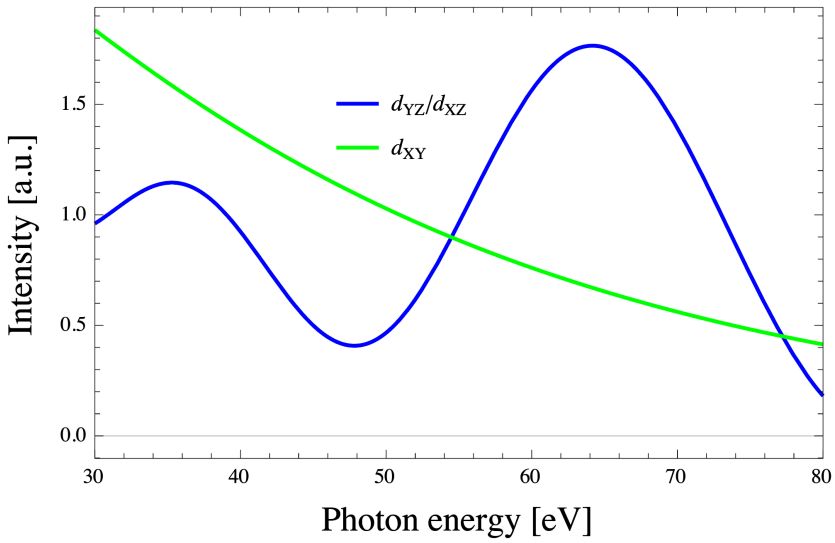

Figure 4.1: Depiction of the expected behaviour for the change in intensity for different photon energies for d_{xy} and $d_{xz,yz}$ bands respectively. This figure is in good agreement with Figure 3.9.

thus been used for the 4d metallic system of Ca_2RuO_4. For illustration see Figure 4.2.

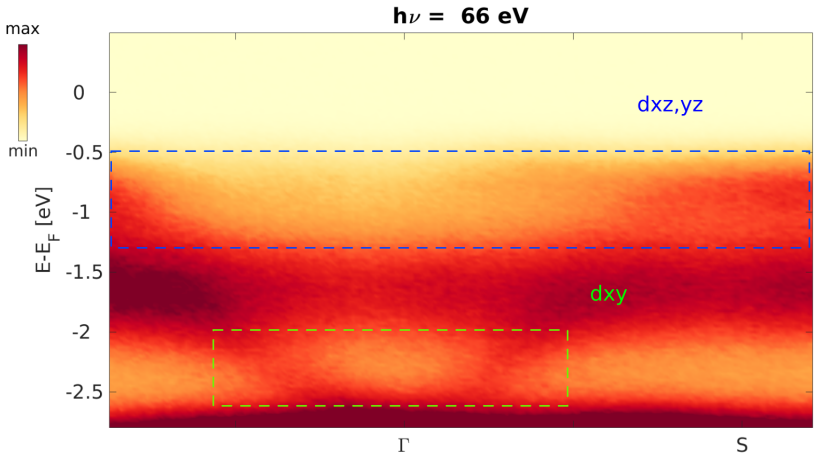

Figure 4.2: ARPES spectrum, taken along Γ-S, with the bands located

Finally it can be concluded that the d_{xy} and $d_{xz,yz}$ bands are subject to different Mott transitions, thus a strong case can be made for orbital selective

Mott physics being the cause for Ca_2RuO_4's insulating state.

Bibliography

[1] A. Einstein, Annalen der Physik **17**, 132 (1905)

[2] V.I. Anisimov *et al.*, Eur. Phys. J. B **25**, 191–201 (2002)

[3] D. Sutter *et al.*, Two Insulating Energy Scales in the Multiband System Ca_2RuO_4, Draft (2016)

[4] M. Braden *et al.*, Phys. Rev. B **58**, 847 (1998)

[5] https://upload.wikimedia.org/wikipedia/commons/5/58/D_orbitals.png (visited: 20.06.2016)

[6] http://www.diamond.ac.uk/Beamlines/Surfaces-and-Interfaces/I05.html (visited: 20.06.2016)

[7] J. Osterwalder, Photoelectron Spectroscopy and Diffraction

[8] A. Damascelli, Physica Scripta Vol. T **109**, 61–74 (2004)

[9] EPO-TEK E4110 Technical Data Sheet

[10] C. Matt, The Pseudo Gap Phase in High Temperature Superconductors, Masterthesis ETH (2012)

[11] X.-P. Wang *et al.*, Phys. Rev. B **85**, 214518 (2012)

[12] E. Gorelov *et al.*, Phys. Rev. Lett. **104**, 226401 (2010)

[13] A. Georges *et al.*, arXiv1207.3033v2 (2012)